Supporting Information

Fluorine-decorated porous Fe-N-C electrocatalysts for proton exchange membrane fuel cells

Rui Gao[a], Zhongyu Qiu[a], Kun Xu[a], Zihui Zhai[a, b], Yuanyuan Cong[c], Qike Jiang[d], Guanghui Zhang[a], Yang Lv [a], Yizheng Guo[a], Yongpeng Li[a], Qingchuan Xu[a], Yi Xiao[a], Yiheng Pang[e], Yun Wang*[e], Yujiang Song*[a]

[a] State Key Laboratory of Fine Chemicals, School of Chemical Engineering, Dalian University of Technology, 2 Linggong Road, Dalian, 116024, China.

[b] School of Mechanical Engineering, Shenyang University, 21 Wanghua South Street, Shenyang 110044, China.

[c] College of Petrochemical Technology, Lanzhou University of Technology, Lanzhou 730050, China.

[d] Instrumentation and Service Center for Physical Sciences, Westlake University, Hangzhou, Zhejiang, 310024, China.

[e.] Mechanical & Aerospace Engineering, University of California, Irvine, CA 92697-3975, USA.

* Corresponding author.

E-mail addresses: yjsong@dlut.edu.cn (Yujiang Song), yunw@uci.edu (Yun Wang),.

Content

1. Materials. ····1

2. Characterizations ····1

3. Electrochemical measurements ····2

4. Calculation of n and H_2O_2 species yields ····3

5. ASD and MSD calculated by nitrite stripping protocol ····4

6. MEAs fabrication and PEMFCs tests ····4

Figure S1 TEM images of house-made ZIF8 (a), F-ZIF8 (b), 15Fe@ZIF8 (c), and F-15Fe@ZIF8 (d). ····5

Figure S2 SEM image and the elemental mappings of C, N, F, and Fe of F-Fe-N-C. ····5

Figure S3 XRD pattern of F-Fe-N-C with references of Fe_3O_4, gamma Fe and $FeN_{0.0324}$. ····5

Figure S4 K-L plot of F-Fe-N-C derived from Fig. 2d. ····6

Figure S5 Electron transfer number of F-Fe-N-C at different loadings on RRDE in 0.1 M $HClO_4$ aq. Inset: corresponding average value of electron transfer number. ····6

Figure S6 Chronoamperometric responses of commercial Pt/C and F-Fe-N-C in O_2-saturated 0.1 M $HClO_4$ aq. with the injection of methanol at about 200 s. ····6

Figure S7 TEM images of F-Fe-N-C synthesized with a hemin content of 5 mg (a), 10 mg (b), 15 mg (c), 20 mg (d), 25 mg (e), and 30 mg (f), respectively. ····7

Figure S8 (a) $E_{1/2}$ and $E_{j=0.1}$ of electrocatalysts synthesized with different molar ratios between 2-TFMI and 2-MI at a loading of 0.6 mg cm^{-2} on RDE (1600 rpm) in 0.1 M $HClO_4$ aq.; (b) A typical photograph of the sample synthesized with pure 2-TFMI. ····7

Figure S9 $E_{1/2}$ and $E_{j=0.1}$ of electrocatalysts synthesized with different pyrolysis temperatures at a loading of 0.6 mg cm^{-2} on RDE (1600 rpm) in 0.1 M $HClO_4$ aq. ····8

Figure S10 N and Fe content of electrocatalysts pyrolyzed at 800, 900, and 1000 °C. ····8

Figure S11 TEM images of samples obtained at 800 °C (a) and 1000 °C (b). ····8

Figure S12 XRD pattens of samples pyrolyzed at 800 and 1000 °C. ····9

Figure S13 Raman spectrum of samples pyrolyzed at 800, 900, and 1000 °C. ····9

Figure S14 Electron transfer number and HO_2^- yield of F-Fe-N-C toward ORR in 0.1 M KOH aq. ····9

Figure S15 Chronoamperometric responses of commercial Pt/C and F-Fe-N-C in O_2-saturated 0.1 M KOH aq. with the injection of methanol at about 200 s. ····10

Figure S16 $E_{1/2}$ and $E_{j=0.1}$ of alkaline ORR of electrocatalysts synthesized with different hemin content (a), varied molar ratio between 2-TFMI and 2-MI (b), and changed pyrolysis temperature (c)

at a loading of 0.6 mg cm^{-2} on RDE (1600 rpm) in 0.1 M KOH aq.; (d) $E_{1/2}$ and $E_{j=0.1}$ of alkaline ORR of F-Fe-N-C at different loadings on RDE (1600 rpm) in 0.1 M KOH aq. ·····10

Figure S17 ORR polarization curves of F-Fe-N-C before and after the addition of 10 mM NaSCN in 0.1 M $HClO_4$ aq. ·····11

Figure S18 N_2 adsorption-desorption isotherms of F-Fe-N-C and house-made Fe-N-C. Inset: pore size distributions. ·····11

Figure S19 (a) High resolution N 1s XPS of F-Fe-N-C; (b) Relative content of different N species of (a). ·····11

Figure S20 Scheme of the components of a PEMFC single cell. ·····12

Figure S21 (a) I-V and power density curves collected under H_2-O_2 and H_2-air conditions; (b-c) Nyquist plots recorded at open circuit voltage under H_2-O_2 and H_2-air conditions; (d) iR-free I-V and power density curves under H_2-O_2 and H_2-air conditions; (e) Tafel plot under H_2-O_2 condition. Note: PEMFC single cells were fabricated with F-Fe-N-C as cathodic CLs. ·····12

Figure S22 PEMFC stability test at 0.55 A cm^{-2} under 1 bar H_2-Air. ·····13

Figure S23 (a) ORR polarization curves of F-Fe-N-C and house-made Fe-N-C in 0.1 M $HClO_4$ aq. with an electrocatalysts loading of 1.2 mg cm^{-2} on RDE at 900 rpm. (b) CVs of house-made Fe-N-C before and after nitrite stripping in 0.5 M acetate buffer aq. ·····13

Figure S24 High resolution C 1s XPS of F-Fe-N-C. ·····13

Figure S25 SEM image of F-Fe-N-C powders with selected areas used for EELS analysis. ·····14

Table S1 Acidic $E_{1/2}$ comparison between F-Fe-N-C and reported electrocatalysts ·····15

Table S2 Acidic MA comparison between F-Fe-N-C and reported electrocatalysts ·····16

Table S3 Alkaline $E_{1/2}$ comparison between F-Fe-N-C and reported electrocatalysts ·····17

Table S4 Fitting data of EXAFS of F-Fe-N-C ·····18

Table S5 ^{57}Fe Mössbauer fitting parameters of F-Fe-N-C ·····18

Table S6 BET analysis of F-Fe-N-C and house-made Fe-N-C ·····18

Table S7 MSD of F-Fe-N-C and reported electrocatalysts ·····19

Table S8 Atomically dispersed Fe loading of F-Fe-N-C and reported electrocatalysts ·····20

Table S9 F content of F-Fe-N-C according to EELS analysis ·····21

Table S10 Structural parameters of MEAs ·····21

Reference ·····22

1. Materials.

2-methylimidazole (2-MI, 99%) and hemin (95%) were obtained from J&K Scientific Ltd (China). Zinc acetate (≥99.0%), polyvinylpyrrolidone (PVP, average mol. wt. 40,000), perchloric acid (70 % $HClO_4$, 99.999% trace metals basis), sodium acetate trihydrate (≥99%) and acetic acid (≥99.7%) were purchased from Sigma-Aldrich (US). Trifluoromethyl imidazole (2-TFMI, 97%) was received from Bide Pharmatech Ltd (China). N, N-dimethylformamide (DMF, ≥99.5% AR) and sodium sulfocyanate (NaSCN, ≥98.5% AR) were ordered from Tianjin Kemiou Chemical Reagent Co. Ltd (China). Ethanol (≥99.8%) and potassium hydroxide (KOH, ≥85% AR) were received from Sinopharm Chemical Reagent Co. Ltd (China). Sodium nitrite ($NaNO_2$, 99.999% metals basis) was obtained from Aladdin Industrial Co (China). Commercial Pt/C (20 wt%, 60 wt%) was received from Johnson Matthey Chemical Co. Ltd (UK). Nafion 211 membrane (~25.4 μm) and Nafion resin solution (5 wt%) were obtained from DuPont (US). Gas diffusion layer (GDL, ~0.4875 mm) was obtained from Sunrise Power Co. Ltd (China). All the above chemicals were used as received without further purification. The ultrapure water (18.2 MΩ cm at 25 °C) was produced from a Millipore water system (Synergy® UV, France) and used in all experiments.

2. Characterizations

Transmission electron microscope (TEM) was carried out on a Tecnai G2 F30 Spirit (FEI) or a HT7700 (Hitachi). High-resolution scanning TEM (HR-STEM), HAADF-STEM, and energy dispersive spectroscopy (EDS) were operated on a JEM-ARM200F (JEOL). Scanning electron microscope (SEM), corresponding EDS, and electron energy loss spectroscopy (EELS) were performed on a SU5000 (Hitachi) or a JSM-7900F (JEOL). Membrane electrode assembly (MEA) was freeze-fractured in liquid nitrogen before SEM analysis. Inductively coupled plasma-optical emission spectrometry (ICP-OES) was carried out on an AVIO 500 (PerkinElmer). Prior to ICP-OES tests, F-Fe-N-C powders were treated at 800 °C in dry air, and then dissolved in an acidic solution. X-ray diffraction (XRD) was recorded on a SmartLab 9 kW (Rigaku) operating at 45 kV and 200 mA. X-ray photoelectron spectroscopy (XPS) was collected on an ESCALAB XI+ (Thermo Scientific) with monochromatized Al Kα (1486.6 eV) as the photon source. A neutralizer was used for the XPS measurements and surface sp^2 C (C-H bond) was used to carry out the calibration. The N content was analyzed with a UNICUBE elemental analyzer (Elementar Analysensysteme). Raman spectra were collected using an inVia Qontor (Renishaw) with an excitation wavelength of 532 nm. N_2 adsorption-desorption isotherm was performed on a Quadrasorb SI (Quantachrome). Specific surface area and pore size distribution were determined by applying the Brunauer-Emmett-Teller (BET) method to analysing the desorption branch. The XAS (Fe K-edge) was collected with BL14W1 beamline

at Shanghai Synchrotron Radiation Facility (SSRF). Fe foil was used as reference to calibrate the energy. The XAS data were analysed by ATHENA, ARTEMIS, and HEPHAESTUS software [1] to gain X-ray absorption near-edge structure (XANES) and extended X-ray absorption fine structure (EXAFS). Wavelet transform (WT) plots [2] were obtained by HamaFortran software [3] with Morlet wavelet equation. ^{57}Fe Mössbauer spectrum was carried out in low field and recorded on a WSS-10 spectrometer with a proportional counter. ^{57}Co(Rh) at a constant acceleration mode was used as the radioactive source. The Doppler velocity of the spectrometer was calibrated with respect to α-Fe at 298 K. MIP was performed with MicroActive AutoPore V 9600 (Micromeritics). For MIP measurements, the electrocatalyst ink was sprayed on a plastic plate instead of membrane to form the CL. Next, the CL was covered by another plastic plate and hot-pressed under 4.6 MPa for 2 min at 130 °C. After being cooled down to room temperature naturally, the top plate was gently removed and the exposed CL is ready for analysis. Totally, five CLs were used for MIP measurements.

3. Electrochemical measurements

A CHI760E electrochemical workstation (Shanghai Chenhua Instruments Ltd.) was used to assess electrocatalysts with a glassy carbon rotating disk electrode (RDE, 5 mm in diameter) as the working electrode (WE), a carbon rod as the counter electrode (CE), and a saturated calomel electrode (SCE, Hg/Hg_2Cl_2 with saturated KCl) or Hg/HgO (1 M NaOH) as the reference electrode (RE), respectively. For the SCE, a salt bridge (agar impregnated with saturated KNO_3) was used to connect the SCE with 0.1 M $HClO_4$ aq. [4]. 8 mg of each NPME was dispersed in the mixture of ultrapure water (98.4 μL), ethanol (885.6 μL), and polyperfluorosulfonic acid (PFSA) resin solution (5 wt%, 16 μL), followed by 15 min of mild sonication to obtain the ink. The loading of NPMEs on RDE ranges from 0.2 to 1.4 mg cm^{-2}. For comparison, 3 mg of commercial Pt/C (20 wt%) was dispersed in the mixture of ultrapure water (300 μL), ethanol (2700 μL), and PFSA resin solution (5 wt%, 18 μL), followed by 5 min of mild sonication to obtain the ink. The Pt loading on RDE is about 10 μg_{Pt} cm^{-2}.

All of the electrochemical tests with RDE were performed in 0.1 M $HClO_4$ or 0.1 M KOH aq. at 25 °C unless otherwise stated. Cyclic voltammetry (CV) tests between 0-1.2 V (vs. RHE) with a scanning rate of 50 mV s^{-1} were performed to clean the surface of electrocatalysts. Linear sweep voltammetry (LSV) was recorded with a positive sweep rate of 10 mV s^{-1}. ORR polarization curves were calibrated by subtracting N_2-saturated LSV from O_2-saturated one. Mass activity (MA) is calculated according to the Koutecky-Levich (K-L) equation:

$$\frac{1}{j} = \frac{1}{j_L} + \frac{1}{j_K} \qquad \text{(S1)}$$

$$MA = \frac{j_K}{m_{catal}} \quad (S2)$$

where j is the collected current density; j_L is the limited diffusion current density; j_K is the kinetic current density; m_{catal} is the electrocatalyst loading on RDE.

Methanol tolerance was evaluated at 0.8 V (vs. RHE) with an amperometric i-t curve by injecting 10 vol% methanol into the electrolyte at approximately 200 s. Durability test was operated by potential cycling from 0.6 to 1.0 V (vs. RHE) for 10,000 cycles at a scanning rate of 100 mV s^{-1}. SCN^- poisoning measurement was carried out in 0.1 M $HClO_4$ aq. in the presence of 10 mM NaSCN. Nitrite poisoning measurement was carried out according to a nitrite stripping protocol with 0.5 M acetate buffer aq. (pH=5.2) as the electrolyte [5]. The RDE coated with 0.27 mg cm^{-2} of F-Fe-N-C was poisoned by 125 mM of $NaNO_2$. Rotating ring-disk electrode (RRDE, 0.2475 cm^2 of disk area, 0.1866 cm^2 of Pt ring area) tests were performed with a positive sweep rate of 10 mV s^{-1} for the disk electrode and a ring potential held at 1.2 V (vs. RHE).

4. Calculation of n and H_2O_2 species yields

To calculate n, the LSV curves were recorded at rotating rates of 400, 625, 900, 1225, 1600, 2025, and 2500 rpm and further fitted with K-L equation (equation S3):

$$\frac{1}{j} = \frac{1}{j_L} + \frac{1}{j_K} = \frac{1}{B}\omega^{-1/2} + \frac{1}{j_K} \quad (S3)$$

where ω is the rotation rate, rpm. B is determined from the slope of K-L plots.

The electron transfer number (n) is obtained according to Levich equation (S4):

$$B = 0.62nFC_0(D_0)^{2/3}(\nu)^{-1/6} \quad (S4)$$

where F is the Faraday constant, 96485 C mol^{-1}; C_0 is the bulk concentration of O_2, 1.26×10^{-6} mol cm^{-3} in 0.1 M $HClO_4$ aq., 1.2×10^{-6} mol cm^{-3} in 0.1 M KOH aq.; D_0 is the diffusion coefficient of O_2, 1.93×10^{-5} cm^2 s^{-1} in 0.1 M $HClO_4$ aq., 1.9×10^{-5} cm^2 s^{-1} in 0.1 M KOH aq.; ν is the kinetic viscosity, 0.01 cm^2 s^{-1} for both 0.1 M $HClO_4$ aq. and 0.1 M KOH aq. [6, 7]. The constant 0.62 is adopted when the rotation speed is expressed in rad s^{-1}.

Since the rotation rate is measured in rpm, the constant number 0.62 should be changed as follow: 0.62 (rad s^{-1})$^{-1/2}$=0.62 (60/2π rpm)$^{-1/2}$=0.2006 $rpm^{-1/2}$. We use the case of 0.1 M $HClO_4$ aq. as an example, $B=0.2006n\times96485\times(1.26\times10^{-6})\times(1.93\times10^{-5})^{2/3}\times(0.01)^{-1/6}=3.781\times10^{-5}n$. Set $\frac{1}{B}=K$, then $n=\frac{1}{(3.781\times10^{-5})K}$. Thus, for the unit of J is mA cm^{-2}, $n=\frac{1}{0.03781K}$. As for 0.1 M KOH aq., $n=\frac{1}{0.03564K}$.

Additionally, n and H_2O_2 species yields can be calculated based on RRDE results:

$$n = 4 \times \frac{I_D}{I_D + I_R/N} \quad \text{(S5)}$$

$$H_2O_2 \text{ species } \% = \frac{200I_R/N}{I_D + I_R/N} \quad \text{(S6)}$$

where I_D is disk current; I_R is ring current; N is the current collection efficiency of the Pt ring. Herein, we use the value of 37% suggested by the provider.

5. ASD and MSD calculated by nitrite stripping protocol

ASD and MSD are calculated according to equation (S7-8):

$$ASD = \frac{Q_{strip} \times N_A}{n_{strip} \times F \times SA} \quad \text{(S7)}$$

$$MSD = \frac{Q_{strip}}{n_{strip} \times F} \quad \text{(S8)}$$

where ASD is areal site density; MSD is mass site density; Q_{strip} is the total charge associated with the NO stripping peak; N_A is the Avogadro constant; n_{strip} is electron transfer number to reduce one adsorbed NO per site; F is the Faraday constant; SA is external surface area of the electrocatalyst (Fig. S18 and Table S6).[5]

6. MEAs fabrication and PEMFCs tests

As-synthesized NPMEs (16 mg) were mixed with ultrapure water (56 μL), ethanol (3600 μL), and PFSA resin solution (5 wt%, 334 μL) under mild sonication for 30 min to prepare cathodic catalyst ink. Similarly, commercial Pt/C (60 wt%, 1.33 mg) was dispersed in the mixture of ultrapure water (57.9 μL), ethanol (598 μL), and PFSA resin solution (5 wt%, 8.5 μL) under sonication to prepare anodic catalyst ink. The cathodic and anodic ink was sprayed to each side of membrane with an active area of 4 cm^2 to attain a cathodic and anodic catalyst loading of 2 mg cm^{-2} and 0.1 mg_{Pt} cm^{-2}, respectively. Finally, the catalyst coated membrane was sandwiched in-between two pieces of gas diffusion layer (GDL) under a pressure of 4.6 MPa for 2 min at 130 °C.

MEAs were assembled in a house-made single cell hardware equipped with a single serpentine flow field at a torque of 4.5 N m. PEMFCs were firstly conditioned under N_2 at 100% relative humidity (RH) until the cell temperature reached 80 °C. Afterwards, the anode and the cathode was supplied with H_2 at 200 mL min^{-1} and O_2 at 300 mL min^{-1} or air at 400 mL min^{-1} at 100 RH%, respectively. Electrochemical impedance spectroscopy (EIS) was carried out at open circuit potential (OCP) by applying an AC amplitude of 10 mV over the AC frequency range from 10 kHz to 100 Hz on an Autolab potentiostat/galvanostat (Echo Chemie BV Model PGSTAT-302N).

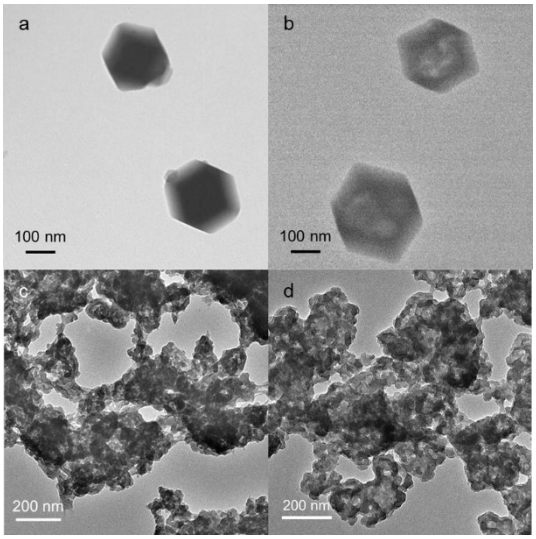

Figure S1 TEM images of house-made ZIF8 (a), F-ZIF8 (b), 15Fe@ZIF8 (c), and F-15Fe@ZIF8 (d).

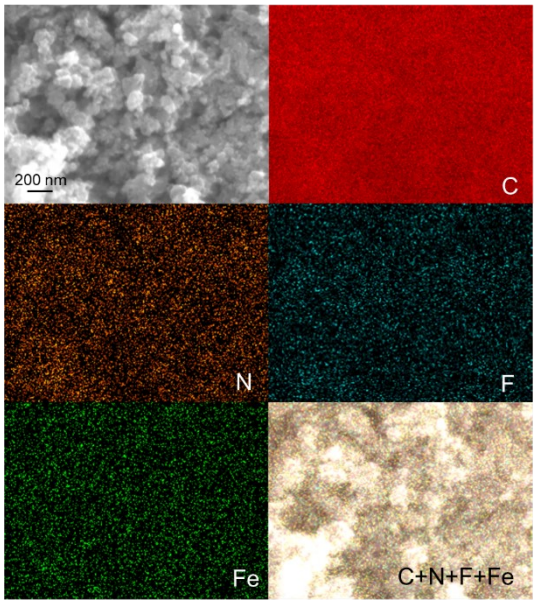

Figure S2 SEM image and the elemental mappings of C, N, F, and Fe of F-Fe-N-C.

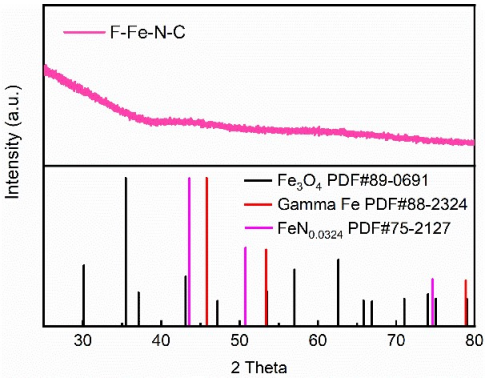

Figure S3 XRD pattern of F-Fe-N-C with references of Fe_3O_4, gamma Fe and $FeN_{0.0324}$.

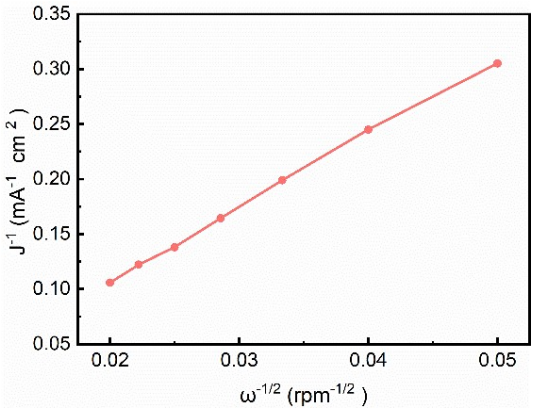

Figure S4 K-L plot of F-Fe-N-C derived from Fig. 2d.

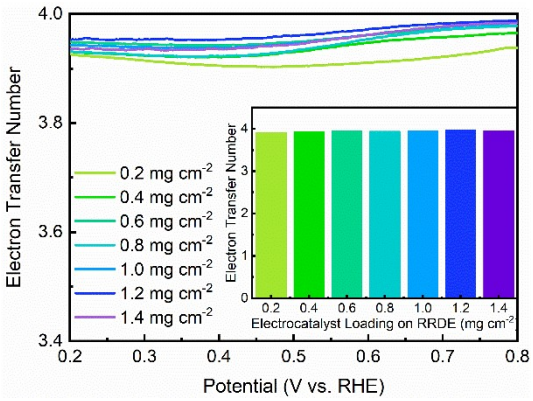

Figure S5 Electron transfer number of F-Fe-N-C at different loadings on RRDE in 0.1 M $HClO_4$ aq. Inset: corresponding average value of electron transfer number.

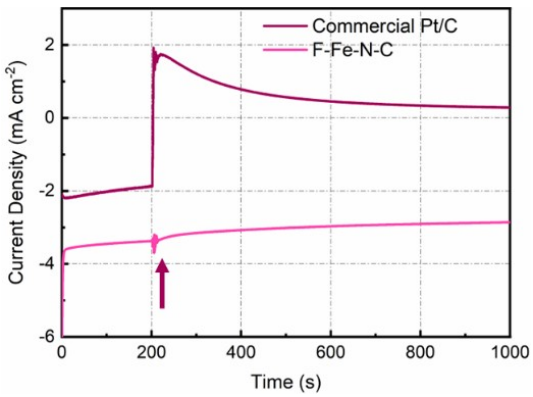

Figure S6 Chronoamperometric responses of commercial Pt/C and F-Fe-N-C in O_2-saturated 0.1 M $HClO_4$ aq. with the injection of methanol at about 200 s.

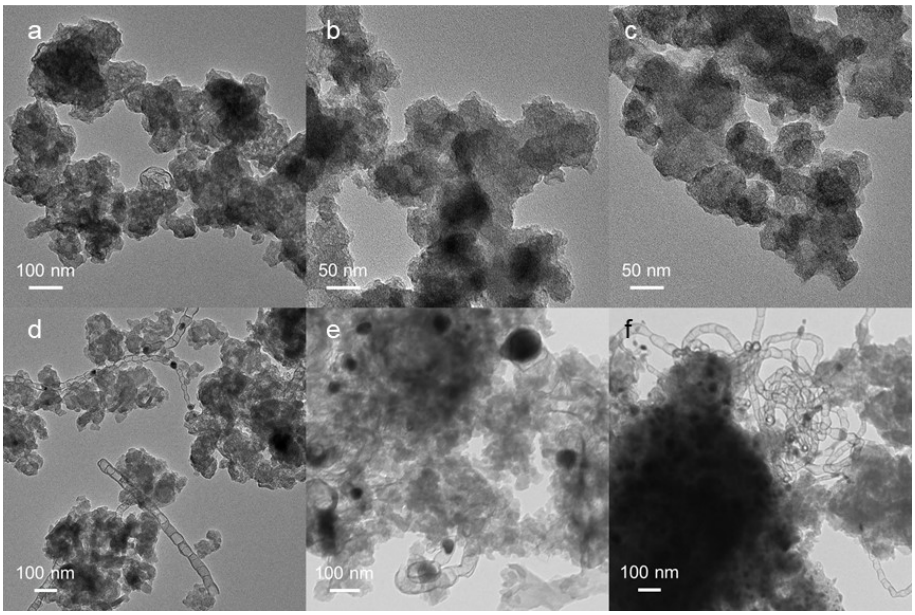

Figure S7 TEM images of F-Fe-N-C synthesized with a hemin content of 5 mg (a), 10 mg (b), 15 mg (c), 20 mg (d), 25 mg (e), and 30 mg (f), respectively.

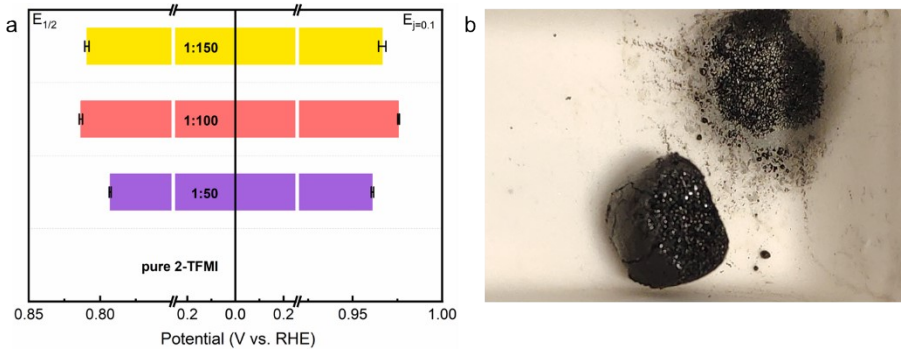

Figure S8 (a) $E_{1/2}$ and $E_{j=0.1}$ of electrocatalysts synthesized with different molar ratios between 2-TFMI and 2-MI at a loading of 0.6 mg cm^{-2} on RDE (1600 rpm) in 0.1 M $HClO_4$ aq.; (b) A typical photograph of the sample synthesized with pure 2-TFMI.

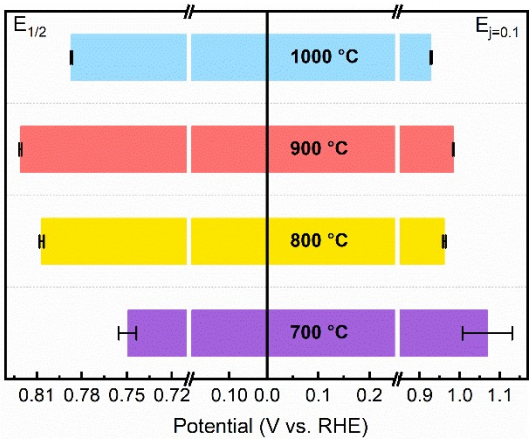

Figure S9 $E_{1/2}$ and $E_{j=0.1}$ of electrocatalysts synthesized with different pyrolysis temperatures at a loading of 0.6 mg cm^{-2} on RDE (1600 rpm) in 0.1 M $HClO_4$ aq.

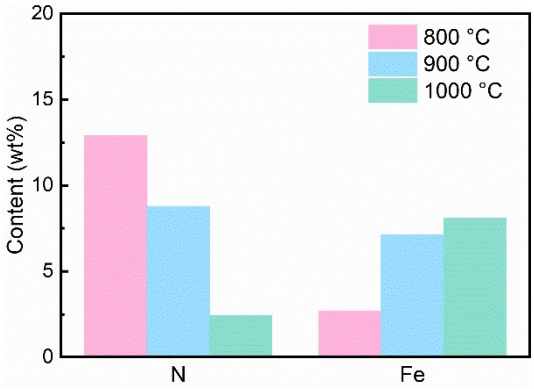

Figure S10 N and Fe content of electrocatalysts pyrolyzed at 800, 900, and 1000 °C.

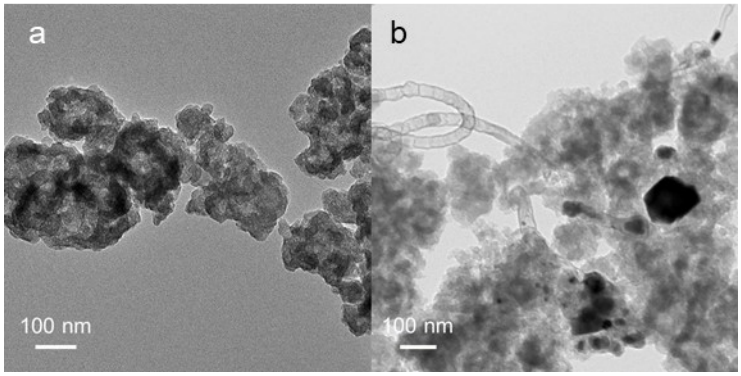

Figure S11 TEM images of samples obtained at 800 °C (a) and 1000 °C (b).

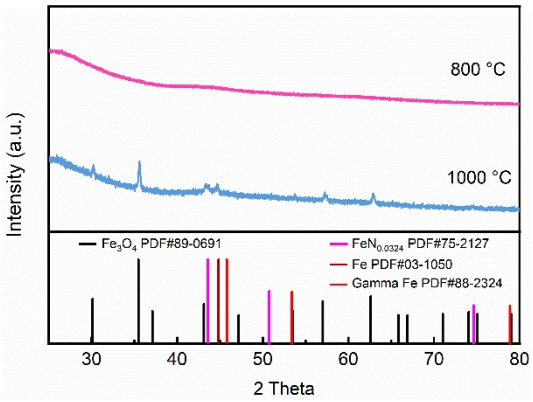

Figure S12 XRD pattens of samples pyrolyzed at 800 and 1000 °C.

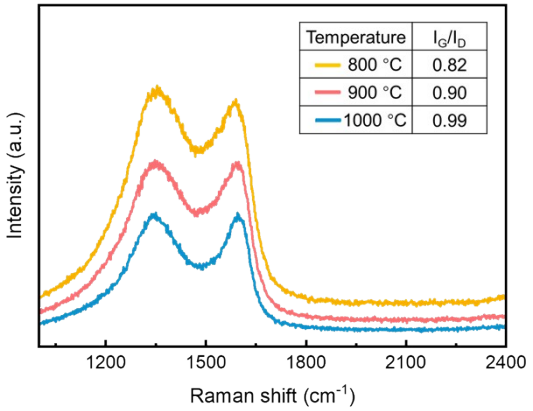

Figure S13 Raman spectrum of samples pyrolyzed at 800, 900, and 1000 °C.

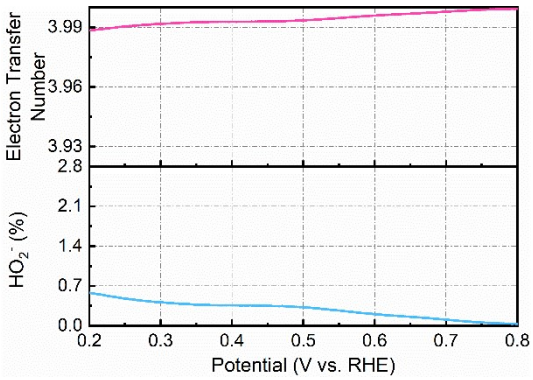

Figure S14 Electron transfer number and HO_2^- yield of F-Fe-N-C toward ORR in 0.1 M KOH aq.

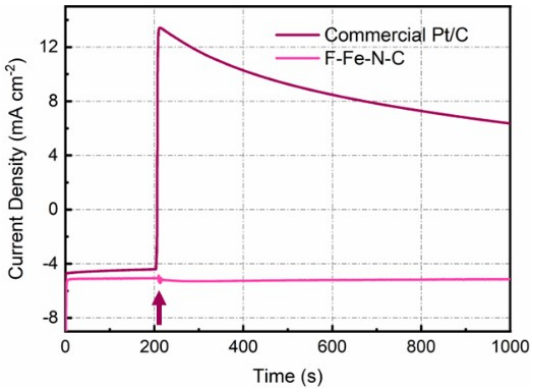

Figure S15 Chronoamperometric responses of commercial Pt/C and F-Fe-N-C in O_2-saturated 0.1 M KOH aq. with the injection of methanol at about 200 s.

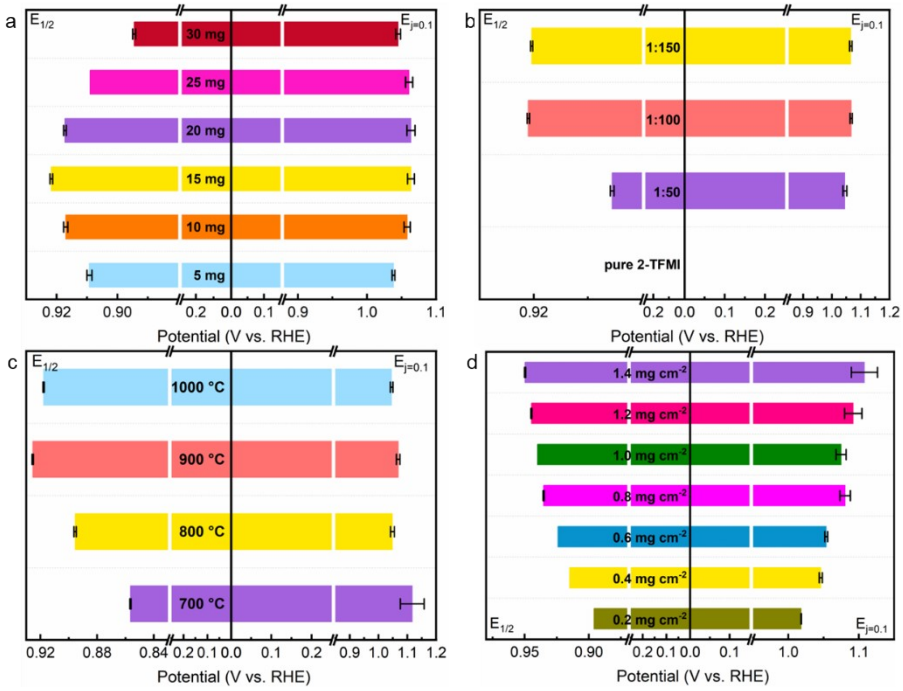

Figure S16 $E_{1/2}$ and $E_{j=0.1}$ of alkaline ORR of electrocatalysts synthesized with different hemin content (a), varied molar ratio between 2-TFMI and 2-MI (b), and changed pyrolysis temperature (c) at a loading of 0.6 mg cm^{-2} on RDE (1600 rpm) in 0.1 M KOH aq.; (d) $E_{1/2}$ and $E_{j=0.1}$ of alkaline ORR of F-Fe-N-C at different loadings on RDE (1600 rpm) in 0.1 M KOH aq.

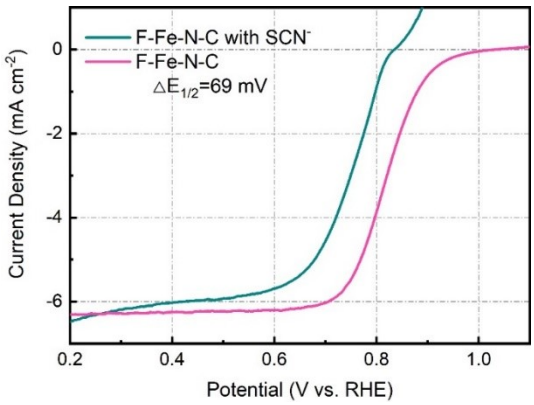

Figure S17 ORR polarization curves of F-Fe-N-C before and after the addition of 10 mM NaSCN in 0.1 M $HClO_4$ aq.

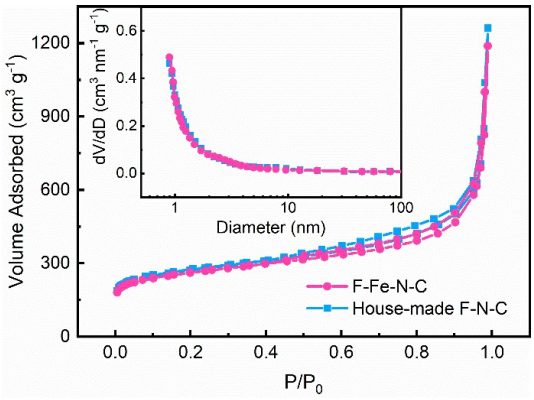

Figure S18 N_2 adsorption-desorption isotherms of F-Fe-N-C and house-made Fe-N-C. Inset: pore size distributions.

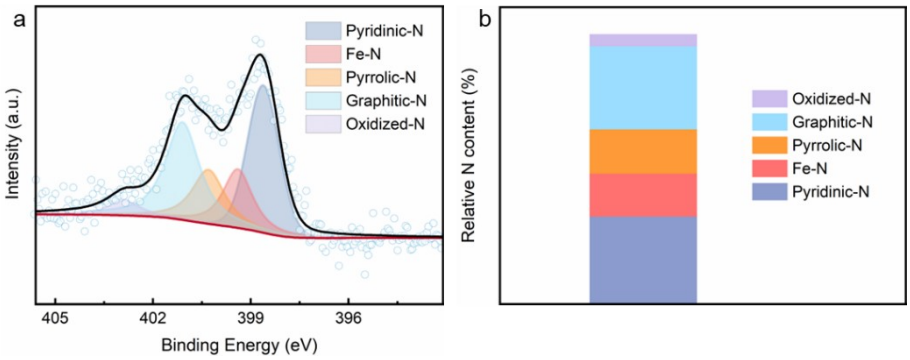

Figure S19 (a) High resolution N 1s XPS of F-Fe-N-C; (b) Relative content of different N species of (a).

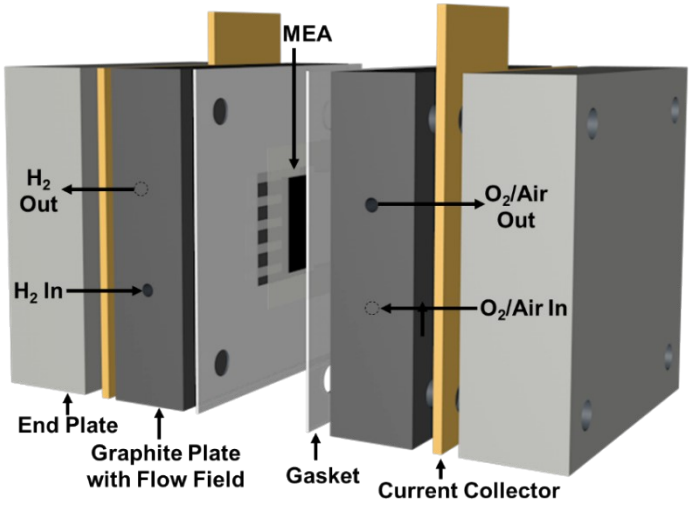

Figure S20 Scheme of the components of a PEMFC single cell.

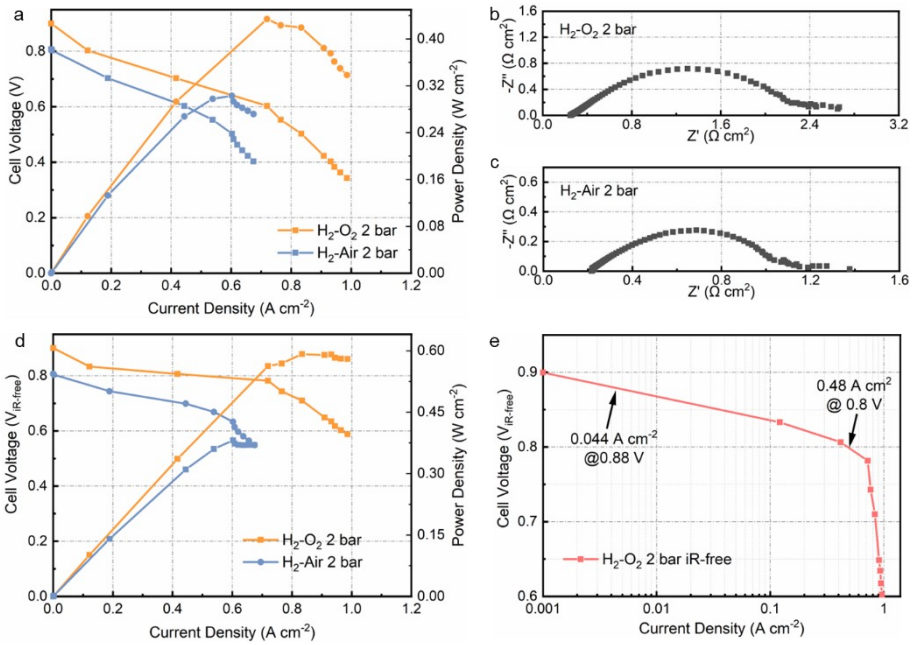

Figure S21 (a) I-V and power density curves collected under H_2-O_2 and H_2-air conditions; (b-c) Nyquist plots recorded at open circuit voltage under H_2-O_2 and H_2-air conditions; (d) iR-free I-V and power density curves under H_2-O_2 and H_2-air conditions; (e) Tafel plot under H_2-O_2 condition. Note: PEMFC single cells were fabricated with F-Fe-N-C as cathodic CLs.

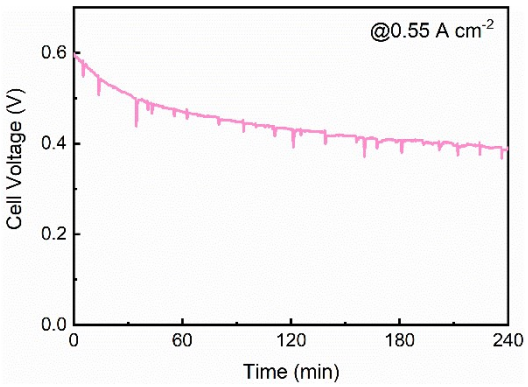

Figure S22 PEMFC stability test at 0.55 A cm^{-2} under 1 bar H_2-Air.

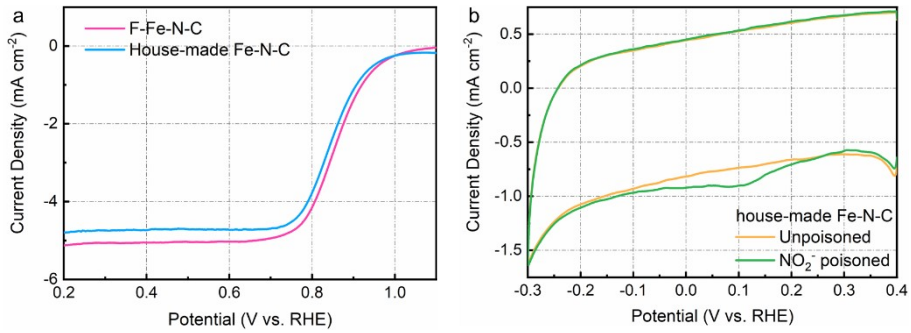

Figure S23 (a) ORR polarization curves of F-Fe-N-C and house-made Fe-N-C in 0.1 M $HClO_4$ aq. with an electrocatalysts loading of 1.2 mg cm^{-2} on RDE at 900 rpm. (b) CVs of house-made Fe-N-C before and after nitrite stripping in 0.5 M acetate buffer aq.

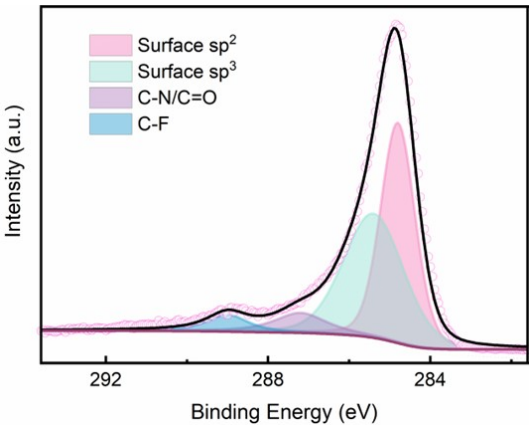

Figure S24 High resolution C 1s XPS of F-Fe-N-C.

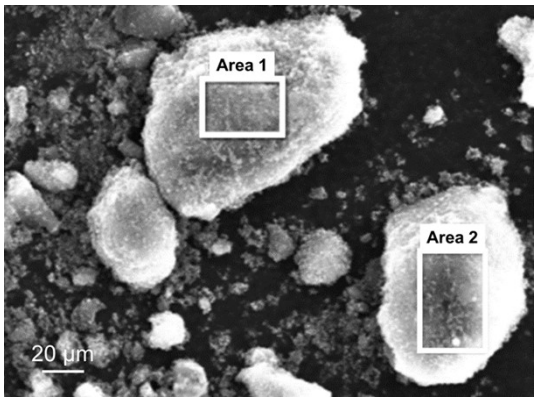

Figure S25 SEM image of F-Fe-N-C powders with selected areas used for EELS analysis.

Table S1 Acidic $E_{1/2}$ comparison between F-Fe-N-C and reported electrocatalysts

Sample	Electrolyte	$E_{1/2}$ (V vs. RHE)	Ref.
F-Fe-N-C	0.1 M $HClO_4$	0.858	This work
Fe-SAs/NPS-HC	0.5 M H_2SO_4	0.791	8
Fe-Nx-CNF	0.1 M $HClO_4$	0.72	9
Fe_{SA}-N-C	0.1 M $HClO_4$	0.80	10
C@PVI-(DFTPP)Fe-800	0.1 M $HClO_4$	0.7	11
NFC@Fe/Fe_3C-9	0.1 M $HClO_4$	0.73	12
CeF_3-Fe/N/C	0.5 M H_2SO_4	0.78	13
MPCo-950-5	0.1 M $HClO_4$	0.69	14
F-FeNC-2	0.5 M H_2SO_4	0.83	15
1.5Fe-ZIF	0.5 M H_2SO_4	0.88	16
Cr/N/C	0.1 M $HClO_4$	0.773	17
FePhenMOF-$ArNH_3$	0.1 M $HClO_4$	0.78	18
1.6%CoNC-$ArNH_3$	0.5 M H_2SO_4	0.785	19
Fe/Ni-N_x/OC	0.1 M $HClO_4$	0.84	20
Fe(Zn)-N-C	0.1 M $HClO_4$	0.83	21

Table S2 Acidic MA comparison between F-Fe-N-C and reported electrocatalysts

Sample	Electrolyte	MA at 0.8 V (A g^{-1})	Ref.
F-Fe-N-C	0.1 M $HClO_4$	19.2	This work
CNRS-RP	0.1 M H_2SO_4	~5	22
UCI-2	0.1 M H_2SO_4	~3.8	22
UCI-1	0.1 M H_2SO_4	2.14	22
sur-FeN_4-HPC	0.1 M $HClO_4$	16.5	23
Fe_2N_6	0.5 M H_2SO_4	8.48	24
d-SA-FeNC	0.5 M H_2SO_4	10.48	25
[Fe(NCs)]_950	0.1 M $HClO_4$	1.22	26
$FeCl_3$-R/M=2/2	0.05 M H_2SO_4	3.0	27
OM-Fe-N-C-steam-800	0.1 M $HClO_4$	12	28

Table S3 Alkaline $E_{1/2}$ comparison between F-Fe-N-C and reported electrocatalysts

Sample	Electrolyte	$E_{1/2}$ (V vs. RHE)	Ref.
F-Fe-N-C	0.1 M KOH	0.956	This work
Fe-SAs/NPS-HC	0.1 M KOH	0.894	8
Fe-Nx-CNF	0.1 M KOH	0.875	9
Fe_{SA}-N-C	0.1 M KOH	0.90	10
Fe/NG-SAC	0.1 M KOH	0.89	29
FeCu-DA/NC	0.1 M KOH	0.86	30
FeCl1N4/CNS	0.1 M KOH	0.921	31
Fe SAs-N/C-20	0.1 M KOH	0.915	32
Fe-N/GNs	0.1 M KOH	0.903	33
FeAB-O	0.1 M KOH	0.9	34
Fe/Ni-Nx/OC	0.1 M KOH	0.938	20
Zn/Fe_2-N-C	0.1 M KOH	0.86	35

Table S4 Fitting data of EXAFS of F-Fe-N-C

Sample	CN	R (Å)	σ^2 (Å^2)	ΔE (eV)	R-factor
F-Fe-N-C	6	1.99	0.01243	-3.188	0.0040928

Table S5 ^{57}Fe Mössbauer fitting parameters of F-Fe-N-C

	IS (mm s^{-1})	QS (mm s^{-1})	Γ (mm s^{-1})	Area (%)	Valence-state
Doublet1	0.42	1.89	1.14	39.6	$Fe^{II}N_4C_{10}$ Low spin
Doublet2	0.38	0.86	0.49	60.4	$Fe^{III}N_4C_{12}$ High spin

Table S6 BET analysis of F-Fe-N-C and house-made Fe-N-C

Samples	Specific Surface Area (m^2 g^{-1})	Micropore Area (m^2 g^{-1})	External Surface Area (m^2 g^{-1})
F-Fe-N-C	962.29	591.65	370.64
House-made Fe-N-C	1007.67	634.47	373.20

Table S7 MSD of F-Fe-N-C and reported electrocatalysts

Sample	Site density (μmol g^{-1})	Ref.
F-Fe-N-C	29.4	This work
FeSMC50	15.3	36
Fe-N-ox-BP	13.1	37
FeN4/NSC-1	25.3	38
FeNC-1:30	19.5	39
FeNC900-HP-900	18.7	40
Bz-Fe1-NC	26.6	41
Fe/PCNFs-950	23.5	42
Fe-N-C/MA	37.3	43
$Fe\text{-}NC^{\Delta\text{-}DCDA}$	77.5	44

Table S8 Atomically dispersed Fe loading of F-Fe-N-C and reported electrocatalysts

Sample	Atomically dispersed Fe loading (wt%)	Ref.
F-Fe-N-C	7.1	This work
FePhenMOF-ArNH_3	0.5	18
FeNCF-(PVP+ZIF-8)	1.28	45
Fe-SAs/NPS-HC	1.54	8
F-FeNC-2	1.68	15
Fe-AC-CVD	1.7	46
pCNT@$Fe_{1.5}$@GL-NH_3	1.72	47
Fe-Nx-CNF	2.04	9
FeN_4/NSC-1	2.2	38
TPI@Z8(SiO_2)-650-C	2.78	48
Fe_{SA}-N-C	3.46	10
Fe-N-C/MA	3.5	43
Fe-N/C-1/30	3.8	49
Fe-N/C	5.86	50
Fe-$NC^{\Delta\text{-DCDA}}$	7	44

Table S9 F content of F-Fe-N-C according to EELS analysis

Element	Weight Percent (wt%)			Atomic Percent (at%)		
	Area 1	Area 2	Ave.	Area 1	Area 2	Ave.
F	0.7	0.6	0.7	0.5	0.4	0.5

Table S10 Structural parameters of MEAs

MEA	Anode CL	Membrane	Cathode CL
F-Fe-N-C	2.4 μm	20.7 μm	56.4 μm
House-made Fe-N-C	2.2 μm	20.3 μm	55.2 μm

Reference

1. B. Ravel and M. Newville, *J. Synchrotron Radiat.*, 2005, **12**, 537-541.
2. Z. Xia, H. Zhang, K. Shen, Y. Qu and Z. Jiang, *Physica B*, 2018, **542**, 12-19.
3. H. Funke and M. Chukalina, HAMA Fortran Version, https://www.esrf.fr/UsersAndScience/Experiments/CRG/BM20/Software/Wavelets/HAMA, (accessed June 12 2021).
4. Y. Lv, H. Liu, J. Li, J. Chen and Y. Song, *J. Electroanal. Chem.*, 2020, **870**, 114172.
5. D. Malko, A. Kucernak and T. Lopes, *Nat. Commun.*, 2016, **7**, 13285.
6. S. Wang, D. Yu and L. Dai, *J. Am. Chem. Soc.*, 2011, **133**, 5182-5185.
7. J. S. Jirkovsky´, M. Halasab and D. J. Schiffrin, *Phys. Chem. Chem. Phys.*, 2010, **12**, 8042-8052.
8. Y. Chen, S. Ji, S. Zhao, W. Chen, J. Dong, W.-C. Cheong, R. Shen, X. Wen, L. Zheng, A. I. Rykov, S. Cai, H. Tang, Z. Zhuang, C. Chen, Q. Peng, D. Wang and Y. Li, *Nat. Commun.*, 2018, **9**, 5422.
9. W. Miao, F. Huang, X. Shen, S. Li, X. Cao, X. Zhang, J. Yu and X. Dong, *Mater. Chem. Front.*, 2022, **6**, 3213-3224.
10. L. Jiao, R. Zhang, G. Wan, W. Yang, X. Wan, H. Zhou, J. Shui, S.-H. Yu and H.-L. Jiang, *Nat. Commun.*, 2020, **11**, 2831.
11. Y.-M. Zhao, P.-C. Zhang, C. Xu, X.-Y. Zhou, L.-M. Liao, P.-J. Wei, E. Liu, H. Chen, Q. He and J.-G. Liu, *ACS Appl. Mater. Interfaces*, 2020, **12**, 17334-17342.
12. M. Karuppannan, J. E. Park, H. E. Bae, Y.-H. Cho and O. J. Kwon, *Nanoscale*, 2020, **12**, 2542-2554.
13. X. Yin, W. Utetiwabo, S. Sun, Y. Lian, R. Chen and W. Yang, *J. Catal.*, 2019, **374**, 43-50.
14. H. Peng, D. Duan, X. Tan, F. Hu, J. Ma, K. Zhang, F. Xu, B. Li and L. Sun, *ChemElectroChem*, 2019, **7**, 131-138.
15. X. Tao, R. Lu, L. Ni, V. Gridin, S. H. Al-Hilfi, Z. Qiu, Y. Zhao, U. I. Kramm, Y. Zhou and K. Müllen, *Mater. Horiz.*, 2022, **9**, 417-424.
16. H. Zhang, H. T. Chung, D. A. Cullen, S. Wagner, U. I. Kramm, K. L. More, P. Zelenay and G. Wu, *Energy Environ. Sci.*, 2019, **12**, 2548-2558.
17. E. Luo, H. Zhang, X. Wang, L. Gao, L. Gong, TuoZhao, Z. Jin, J. Ge, Z. Jiang, C. Liu and WeiXing, *Angew. Chem. Int. Ed.*, 2019, **58**, 12469-12475.
18. J. Li, S. Ghoshal, W. Liang, M.-T. Sougrati, F. Jaouen, B. Halevi, S. McKinney, G. McCool, C. Ma, X. Yuan, Z.-F. Ma, S. Mukerjee and Q. Jia, *Energy Environ. Sci.*, 2016, **9**, 2418-2432.
19. L. Chen, X. Liu, L. Zheng, Y. Li, X. Guo, X. Wan, Q. Liu, J. Shang and J. Shui, *Appl. Catal. B*, 2019, **256**, 117849.
20. Z. Zhu, H. Yin, Y. Wang, C.-H. Chuang, L. Xing, M. Dong, Y.-R. Lu, G. Casillas-Garcia, Y. Zheng, S. Chen, Y. Dou, P. Liu, Q. Cheng and H. Zhao, *Adv. Mater.*, 2020, **32**, 2004670.
21. L. Gong, H. Zhang, Y. Wang, E. Luo, K. Li, L. Gao, Y. Wang, Z. Wu, Z. Jin, J. Ge, Z. Jiang, C. Liu and W. Xing, *Angew. Chem. Int. Ed.*, 2020, **59**, 13923-13928.
22. K. T. Santos, K. Kumar, L. Dubau, H. Ge, S. Berthon-Fabry, C. S. A. Vasconcellos, F. H. B. Lima, T. Asset, P. Atanassov, V. A. Saveleva, P. Glatzel, X. Li, F. Jaouen and F. Maillard, *J. Power Sources*, 2023, **564**, 232829.
23. G. Chen, Y. An, S. Liu, F. Sun, H. Qi, H. Wu, Y. He, P. Liu, R. Shi, J. Zhang, A. Kuc, U. Kaiser, T. Zhang, T. Heine, G. Wu and X. Feng, *Energy Environ. Sci.*, 2022, **15**, 2619-2628.
24. N. Zhang, T. Zhou, J. Ge, Y. Lin, Z. Du, C. a. Zhong, W. Wang, Q. Jiao, R. Yuan, Y. Tian, W. Chu, C. Wu and Y. Xie, *Matter*, 2020, **3**, 509-521.
25. L. Shi, X. Lin, F. Liu, Y. Long, R. Cheng, C. Tan, L. Yang, C. Hu, S. Zhao and D. Liu, *ACS Catal.*, 2022, **12**, 5397-5406.
26. B. Koyuturk, E. M. Farber, F. E. Wagner, T.-P. Fellinger and D. Eisenberg, *J. Mater. Chem. A*, 2022, **10**, 19859-19867.
27. H. Ge, N. Bibent, K. Teixeira Santos, K. Kumar, J. Jaxel, M.-T. Sougrati, A. Zitolo, M. Dupont, F. Lecoeur, M. Mermoux, V. Martin, L. Dubau, F. Jaouen, F. Maillard and S. Berthon-Fabry, *ACS Catal.*, 2023, **13**, 1149-1163.
28. J. Zou, C. Chen, Y. Chen, Y. Zhu, Q. Cheng, L. Zou, Z. Zou and H. Yang, *ACS Catal.*, 2022, **12**, 4517-4525.
29. M. Xiao, Z. Xing, Z. Jin, C. Liu, J. Ge, J. Zhu, Y. Wang, X. Zhao and Z. Chen, *Adv. Mater.*, 2020, **32**, e2004900.
30. C. Du, Y. J. Gao, H. Q. Chen, P. Li, S. Y. Zhu, J. G. Wang, Q. G. He and W. Chen, *J. Mater. Chem. A*, 2020, **8**, 16994-17001.
31. Y. Han, Y. Wang, R. Xu, W. Chen, L. Zheng, A. Han, Y. Zhu, J. Zhang, H. Zhang, J. Luo, C. Chen,

Q. Peng, D. Wang and Y. Li, *Energy Environ. Sci.*, 2018, **11**, 2348-2352.
32. R. Jiang, L. Li, T. Sheng, G. Hu, Y. Chen and L. Wang, *J. Am. Chem. Soc.*, 2018, **140**, 11594-11598.
33. D. Liu, J. C. Li, S. Ding, Z. Lyu, S. Feng, H. Tian, C. Huyan, M. Xu, T. Li, D. Du, P. Liu, M. Shao and Y. Lin, *Small Methods*, 2020, **4**, 1900827.
34. K. Chen, K. Liu, P. An, H. Li, Y. Lin, J. Hu, C. Jia, J. Fu, H. Li, H. Liu, Z. Lin, W. Li, J. Li, Y.-R. Lu, T.-S. Chan, N. Zhang and M. Liu, *Nat. Commun.*, 2020, **11**, 4173.
35. J. Xue, Y. Li and J. Hu, *J. Mater. Chem. A*, 2020, **8**, 7145-7157.
36. G. Daniel, M. Mazzucato, R. Brandiele, L. D. Lazzari, D. Badocco, P. Pastore, T. Kosmala, G. Granozzi and C. Durante, *ACS Appl. Mater. Interfaces*, 2021, **13**, 42693-42705.
37. J. Müller-Hülstede, D. Schonvogel, H. Schmies, P. Wagner, A. Dyck and M. Wark, *ACS Appl. Energy Mater.*, 2021, **4**, 6912-6922.
38. C. Maouche, J. Yang, S. H. Al-Hilfi, X. Tao and Y. Zhou, *ACS Appl. Nano Mater.*, 2022, **5**, 4397-4405.
39. J. Xu, G. Liang, D. Chen, Z. Li, H. Zhang, J. Chen, F. Xie, Y. Jin, N. Wang and H. Meng, *Appl. Surf. Sci.*, 2022, **573**, 151607.
40. D. Xia, C. Yu, Y. Zhao, Y. Wei, H. Wu, Y. Kang, J. Li, L. Gan and F. Kang, *Chem. Sci.*, 2021, **12**, 11576-11584.
41. D. Wang, Y. Wu, Z. Li, H. Pan, Y. Wang, M. Yang and G. Zhang, *Chem. Eng. J.*, 2021, **424**, 130401.
42. L. Yang, L. Yu, Z.-H. Huang, F. Kang and R. Lv, *J. Energy Chem.*, 2022, **75**, 430-440.
43. Y. Zhou, G. Chen, Q. Wang, D. Wang, X. Tao, T. Zhang, X. Feng and K. Müllen, *Adv. Funct. Mater.*, 2021, **31**, 2102420.
44. A. Mehmood, M. Gong, F. Jaouen, A. Roy, A. Zitolo, A. Khan, M.-T. Sougrati, M. Primbs, A. M. Bonastre, D. Fongalland, G. Drazic, P. Strasser and A. Kucernak, *Nat. Catal.*, 2022, **5**, 311-323.
45. W. Jiang, B. Huang, R. Hu, Y. Cui and L. Guan, *Nanotechnology*, 2022, **33**, 195401.
46. S. Liu, C. Li, M. J. Zachman, Y. Zeng, H. Yu, B. Li, M. Wang, J. Braaten, J. Liu, H. M. Meyer, M. Lucero, A. J. Kropf, E. E. Alp, Q. Gong, Q. Shi, Z. Feng, H. Xu, G. Wang, D. J. Myers, J. Xie, D. A. Cullen, S. Litster and G. Wu, *Nat. Energy*, 2022, **7**, 652-663.
47. S. H. Ahn, X. Yu and A. Manthiram, *Adv. Mater.*, 2017, **29**, 1606534.
48. X. Wan, X. Liu, Y. Li, R. Yu, L. Zheng, W. Yan, H. Wang, M. Xu and J. Shui, *Nat. Catal.*, 2019, **2**, 259-268.
49. W. Wei, X. Shi, P. Gao, S. Wang, W. Hu, X. Zhao, Y. Ni, X. Xu, Y. Xu, W. Yan, H. Ji and M. Cao, *Nano Energy*, 2018, **52**, 29-37.
50. G. Ye, Q. He, S. Liu, K. Zhao, Y. Su, W. Zhu, R. Huang and Z. He, *J. Mater. Chem. A*, 2019, **7**, 16508-16515.